Mechanical Systems and Signal Processing 90 (2017) 189–207

Contents lists available at ScienceDirect

Mechanical Systems and Signal Processing

journal homepage: www.elsevier.com/locate/ymssp

Omnidirectional regeneration (ODR) of proximity sensor signals for robust diagnosis of journal bearing systems

Joon Ha Jung [a], Byung Chul Jeon [a], Byeng D. Youn [a,*], Myungyon Kim [a], Donghwan Kim [b], Yeonwhan Kim [b]

[a] Department of Mechanical and Aerospace Engineering, Seoul National University, Seoul 08826, Republic of Korea
[b] Power Generation Laboratory, KEPCO Research Institute, 34056, Republic of Korea

ARTICLE INFO

Article history:
Received 13 January 2016
Received in revised form 25 October 2016
Accepted 20 December 2016

Keywords:
Journal bearing rotor system
Anomaly diagnosis
Gap sensor
Vibration signal
Directionality of anomaly

ABSTRACT

Some anomaly states of journal bearing rotor systems are direction-oriented (e.g., rubbing, misalignment). In these situations, vibration signals vary according to the direction of the sensors and the health state. This makes diagnosis difficult with traditional diagnosis methods. This paper proposes an omnidirectional regeneration method to develop a robust diagnosis algorithm for rotor systems. The proposed method can generate vibration signals in arbitrary directions without using extra sensors. In this method, signals are generated around the entire circumference of the rotor to consider all possible directions. Then, the directionality of each state is proved by mathematically and is evaluated using a proposed metric. When a directional state is determined, the classification is carried out on all of the generated signals. When a non-directional state is found, the classification is performed on only one of the generated signals to minimize computational load without sacrificing accuracy. The proposed ODR method was validated using experimental data. The classification results show that the proposed method generally outperforms the conventional classification method. The results support the proposed concept of using ODR signals in diagnosis procedures for journal bearing systems.

1. Introduction

Journal bearing rotor systems are frequently used in industrial machines that require safe and reliable operation. For example, turbines and pumps in power plants use journal bearings to maintain system safety even in heavy load and high-speed conditions. Because the fluid in the bearings supports the rotors, stable operation is possible without direct contact between the rotor and the stator. Although a particular rotor system may satisfy all design requirements, uncertainties in operation can cause the system to operate in an unexpected way. Sometimes, improper maintenance can cause a sudden failure or an accident; this can result in disastrous consequences. Thus, to prevent catastrophic events, large rotor systems require an anomaly diagnosis system.

Diagnosis systems for rotors frequently use data-driven methods [1–7]. These methods follow three steps: data acquisition, feature generation, and classification. First, in the data acquisition step, signals from each health state are obtained. Most rotor diagnosis systems use vibration signals, because vibration signals can accurately represent the health state of

* Corresponding author.
E-mail address: bdyoun@snu.ac.kr (B.D. Youn).

http://dx.doi.org/10.1016/j.ymssp.2016.12.030
0888-3270/

Nomenclature

C	regularization parameter of the optimization problem for support vector machine
D	directionality metric of health states
N	number of possible ODR signals by θ
$S(f)$	power spectrum
$S_N(f)$	set of the power spectrum from N ODR signals
V	time signal
$\overline{V}$	mean of the time signal
X_i-Y_i	Cartesian coordinate system by X_i and Y_i axes
b	bias of the hyper-plane
d	dimension of the feature vector
u_i	label of the ith feature vector
$\boldsymbol{v}_i$	ith feature vector
$\boldsymbol{w}$	normal vector to the hyper-plane
θ	angle of rotation
ξ_i	slack variable of ith feature data

the system. Next, the feature generation step is composed of two sub-steps: feature extraction and selection. The acquired data are used to generate key features that should distinguish the health states of the rotor system. Various signal processing techniques have been developed to extract features from the data. Noise reduction, such as time synchronous averaging, can be performed [8,9]. Angular resampling can also reduce the noise, as well as produce an equal number of data points per cycle [10,11]. After these preprocessing techniques are applied, features are extracted. Time- and frequency-domain analysis are widely used methods for feature extraction [12–14]. Time-frequency analysis is another technique specifically for transient signals [15,16]. Hilbert-Huang transform [17], empirical mode decomposition (EMD) [18], and wavelet transform [19] are used to extract features from various rotor systems. After the candidate features are extracted, key features must be selected for robust anomaly detection. Through the feature selection process, the optimal feature subset can be obtained [20–23]. Finally, the classification is performed using machine learning algorithms focused on the selected optimal features. Artificial neural networks (ANN) [14,24], support vector machine (SVM) methods [25–29], linear discriminant analysis (LDA) [25,30], and related techniques can be used for the classification.

Normally, two vibration signals are acquired from two fixed sensors at an axial position in the journal bearing system. However, employing two sensors at fixed orientations may not detect direction-oriented anomalies. For example, an impact rubbing in an arbitrary direction may not be detected by fixed sensors. A simple mathematical model of the rubbing confirms dependency on the orientation of sensors. This underscores the need for the use of omnidirectional signals for robust diagnosis.

Some prior research efforts have tried to consider direction in rotor diagnosis by using the orbit shape and the full-spectrum of vibration signals. Yan et al. [31] modified the orbit into seven different features to identify the state of the steam turbine generator. Wang et al. [32] quantified the orbit information with isometric feature mapping to identify faults in rotors. Other researchers also tried to quantify the orbit shape to make more accurate diagnosis of rotors [33–36]. However, in the process of quantifying the orbit shape, detailed physical interpretation of vibration signals may be diminished. In other work, the full-spectrum of vibration signals was used to see forward and backward whirling frequency components by using x- and y- signals [37–40]; however, the method could not consider vibration signals in all directions.

Thus, to overcome these problems with existing methods, we propose an omnidirectional regeneration (ODR) method that can robustly diagnose rotor health states. The proposed method considers omnidirectional vibration signals without installing extra sensors. While ODR makes use of the basic concepts of conventional, data-driven diagnosis steps, the classification and the feature generation steps are revised. As a result, the ODR method outperforms the conventional method of using signals from fixed sensors. The effectiveness of our proposed approach of considering the directionality of the health state using the ODR method was validated using experimental data from a testbed.

This paper is organized as follows. Section 2 briefly states the experimental setup and provides an overview of conventional, data-driven diagnosis steps. Section 3 presents the proposed ODR-based method with physical interpretation and its procedure. Section 4 shows that the ODR-based method outperforms the conventional one for anomaly diagnosis. A summary of the research is provided in Section 5.

2. Overview of journal bearing rotor diagnosis systems

Supervised-learning methods are the most popular methods used for diagnosis of journal bearing rotor systems. Vibration signals in the rotor systems are commonly used for supervised diagnosis methods. This section provides an overview of supervised-learning methods and our research testbed. Section 2.1 describes the configuration of the testbed and the vibra-

tion signals from the proximity sensors. Section 2.2 provides a brief overview of the overall diagnosis processes used for supervised-learning methods.

2.1. Vibration signals

This research employed vibration signals obtained from an RK4 testbed. The testbed is a journal bearing rotor system product of GE Bently-Nevada. We tested normal conditions and four anomaly conditions, specifically: (1) normal, (2) rubbing, (3) rubbing with unbalance, (4) misalignment, and (5) oil whirl. Section 2.1.1 describes the configuration of the RK4 testbed and the experimental setup for the five health states. Section 2.1.2 presents the acquisition of vibration signals via proximity sensors.

2.1.1. Testbed setup for each health state

The configuration of the RK4 is presented in Fig. 1a. Two shafts of 10 mm diameter—one long shaft and the other short—are supported by three journal bearings. The two shafts are connected by a flexible coupling. The motor and the short shaft are connected by another flexible coupling. The long shaft is supported by two bearings with an 800-gram disc attached to the shaft. Despite the effort to balance the rotor system, a bit of unbalance exists. For the normal state, the amplitude of the vibration signals was set at a 10 μm root-mean squares (rms) level, which was determined from ISO 7919-2 [41]. The misalignment was tested by shifting the shorter shaft 20 μm horizontally. The special jig shown in Fig. 1b was used to control the exact amount of the shift. The rubbing state, precisely impact rubbing, was obtained by adding a rubbing screw to the normal state, as presented in Fig. 1c. Direct contact with the shaft was controlled using the accelerometer attached to the jig. The rubbing was controlled within a 2.0 ± 0.3 m/s^2 range. In addition to the rubbing, rubbing with unbalance was tested as a separate health state. A direct contact was made during an unbalanced state, where a 15 g·mm weight was added to the normal state configuration. The oil whirl state used an additional tool kit for oil whirl, as presented in Fig. 1d. Spring tension and oil pressure were controlled. The oil whirl data were acquired at an oil pressure of 35 kPa.

All health states were tested in a 3600-rpm steady-state condition. For each test, vibration signals were measured through Bently-Nevada 3300 proximity sensors. The sensors were placed in pairs at locations near the 2nd and 3rd bearings, as shown in Fig. 2. In addition, another proximity sensor was mounted at the motor coupling, and the signals obtained from this sensor were used as the keyphasor signal. All proximity signals were measured in a voltage form, where the AC component represents the relative vibration of the shaft and the DC component represents the motion of the centerline of the shaft. The sampling rate was set at 8500 Hz. Three 60-s tests were executed for each health state.

The health states can be grouped into directional and non-directional states. A non-directional health state is defined as a state that possesses signal characteristics irrespective to the orientation of the sensor. In contrast, a directional health state is

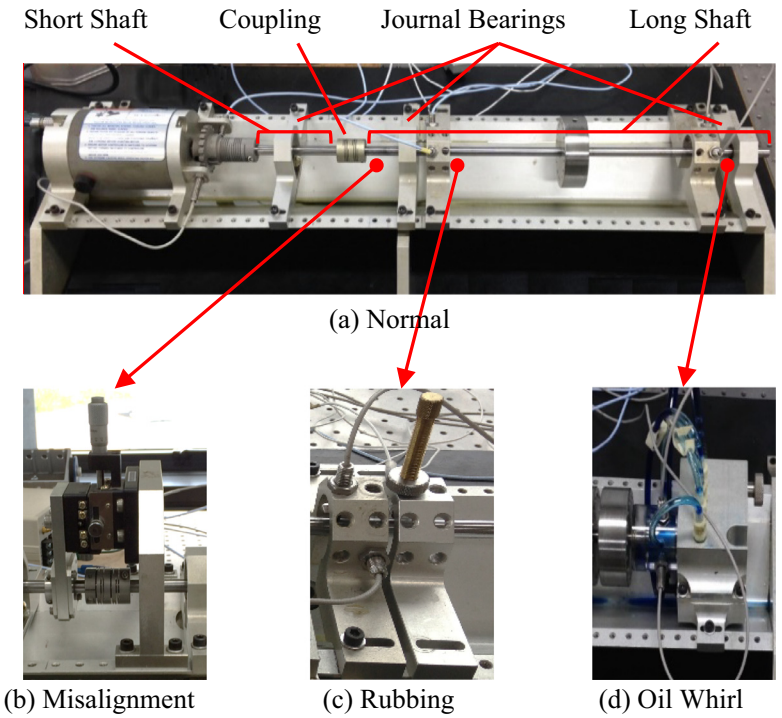

Fig. 1. RK4 testbed setup.

a state with signal characteristics dissimilar to those described for the non-directional state. Normal and oil whirl states are non-directional health states. Misalignment, rubbing, and rubbing with unbalance are directional health states. Section 3.2 will discuss quantitative evaluation of directionality.

2.1.2. Measurement of vibration signals via proximity sensors

In journal bearing rotor diagnosis systems, vibration signals are measured through proximity sensors. The sensors directly measure the motion of the rotating shaft. The vibration signals thus preserve the physical characteristics of the system. These vibration signals are obtained in a voltage form, which is proportional to the gap between the rotor and the sensors. Most journal bearing rotors use proximity sensors in pairs. The paired sensors are installed in a right angle to acquire two independent signals, as shown in Fig. 3. The vibration signal acquired from one sensor can be denoted as the *x*-signal, while the signal from the other sensor can be denoted as the *y*-signal. Since *x*- and *y*-sensors are placed in a right angle, the orbit of the shaft centerline position can be determined using the two signals.

2.2. Diagnosis process based on Supervised-Learning

A supervised learning method is often used for health diagnosis of journal bearing rotor systems. Supervised learning methods train classifiers using labeled data acquired from known states of the system. Then, unknown health states of the system can be predicted using the class (label) of the data. Section 2.2.1 describes the feature generation process; Section 2.2.2 states the SVM algorithm as a classifier used to train and predict the labels.

2.2.1. Feature generation

The feature generation process transforms vibration signals into quantified features. Generally, features that have high separation ability lead to better overall performance of the diagnosis algorithm. To acquire optimal features for the diagnosis system, the feature generation process is separated into three sub-processes—preprocessing, feature extraction, and feature selection.

First, preprocessing reduces the uncertainties of raw vibration signals. The rpm of journal bearing rotors has a slight variation even in steady-state conditions. This variation of rpm causes inconsistency in feature extraction. To reduce the rpm variance, the raw vibration signals are resampled. The angular resampling [42] technique can make the signals have an equal number of points per rotation with reference to the keyphasor signals. The keyphasor signal has one peak per rotation, so the peaks can be regarded as the reference point for each rotation. Within a rotation, raw signals are resampled based on the uniformly distributed phase points.

Second, feature extraction quantifies characteristics of health states. As this research targets a system in a steady-state condition, time- and frequency-domain features are used rather than time-frequency domain features. Eight time-domain and eleven frequency-domain features were chosen, as shown in Table 1 [43]. The eight time-domain features include energy-related features, sinusoidal wave shape related features, and statistical moments of vibration signals. The eleven frequency-domain features contain the change of the main frequency of the vibration and the magnitudes of certain frequency ranges. One-cycle based datum units are used for extracting time-domain features, while sixty-cycle based datum units are used for extracting frequency-domain features [43].

Finally, feature selection determines the optimal subset of the features that leads to enhanced diagnostic performance. Not all of the features have good separation ability, and some features may be redundant. To improve the performance of the diagnosis algorithm, a probability-of-separation (PoS)-based genetic algorithm is used to obtain the optimal set of features [43,44].

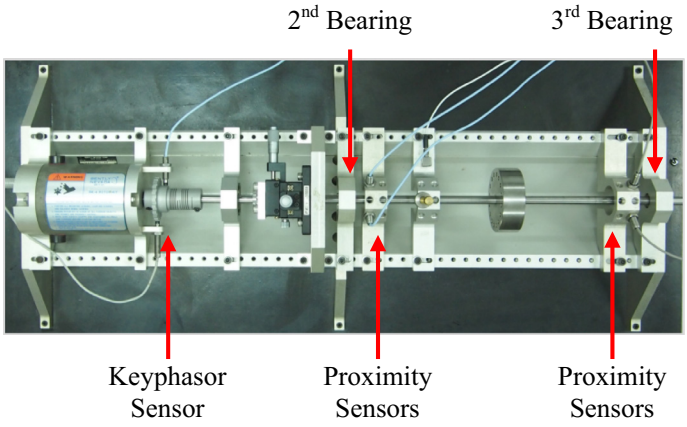

Fig. 2. Location of the sensors.

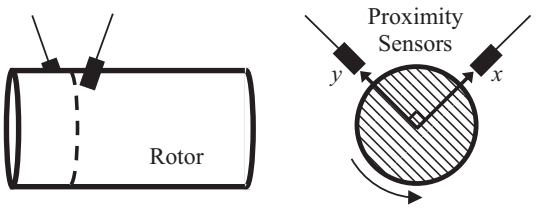

Fig. 3. Proximity sensors in rotor.

2.2.2. Support vector machine (SVM) classification

The classification process involves two steps: training and prediction. In this research, the support vector machine (SVM) algorithm was used for the classification. SVM is a widely used machine learning technique that minimizes structural risk through optimization. Specifically, the decision hyper-plane is found by maximizing the distance between the closest data points from the two classes. The unlabeled data can then be classified using the trained hyper-plane.

For a two-class SVM problem, the training step requires solving a minimization of structural risk problem to obtain a hyper-plane that separates the two classes. The labeled data set, $\{(\boldsymbol{v}_i, u_i)\}$, is used for training the hyper-plane, where $\boldsymbol{v}_i \in \boldsymbol{R}^n$ and $u_i \in \{1, -1\}$. $\boldsymbol{v}_i$ is the d feature vector of ith data, and u_i is the corresponding label. Then, the optimization problem to find the hyper-plane can be defined as follows:

$$\begin{aligned} &\text{minimize} && \frac{\boldsymbol{w}^2}{2} + C\sum_{i=1}^{l}\xi_i \\ &\text{subject to} && u_i(\boldsymbol{w}\cdot\boldsymbol{v}_i - b) \geqslant 1 - \xi_i, \quad i = 1,\ldots,l \\ & && \xi_i \geqslant 0, \qquad\qquad i = 1,\ldots,l \end{aligned} \tag{1}$$

where $\boldsymbol{w}$ is the normal vector to the hyper-plane, b is the bias of the hyper-plane, C is the regularization parameter, ξ_i is the ith slack variable, and l is the number of training vectors. Then, the classes of unlabeled data are predicted using the decision function as follows:

$$\text{sgn}(\boldsymbol{w}\cdot\boldsymbol{v} + b) \tag{2}$$

where $\boldsymbol{v}$ denotes the feature vector of unlabeled test data. To solve the multi-class problem, a one-against-all method [45] was used in this research. The SVM problems were solved using the LIBSVM code [46].

3. Omnidirectional regeneration (ODR) for diagnosis of directional faults

This section introduces a newly proposed diagnosis algorithm that overcomes the fixed orientations of the sensors. Section 3.1 defines the omnidirectional regeneration (ODR) of the vibration signals, validates the ODR signals, and provides the physical interpretation of the ODR method. In Section 3.2, a metric for directionality evaluation is proposed to categorize the health states as either directional or non-directional. Section 3.3 presents how ODR signals are used in the diagnosis process.

Table 1
(a) Time-domain features and (b) frequency-domain features.

	Features	Description		Features	Description
Energy related	Max.	$\text{Max}(\lvert\boldsymbol{V}\rvert)$	Main frequency related	FC	$\int f \times S(f)df / \int S(f)df$
	Mean	$\text{Mean}(\lvert\boldsymbol{V}\rvert)$		RMSF	$\sqrt{\int f^2 \times S(f)df / \int S(f)df}$
	RMS	$\sqrt{\frac{1}{k}\sum_{i=1}^{k}\lvert V_i\rvert^2}$		RVF	$\sqrt{\int (f - FC)^2 \times S(f)df / \int S(f)df}$
Statistical moment related	Skewness	$\sum (V_i - \overline{\boldsymbol{V}})^3/\sigma^3$		0.5X/1X	$\sqrt{S(f_{0.5X})/S(f_{1X})}$
	Kurtosis	$\sum (V_i - \overline{\boldsymbol{V}})^4/\sigma^4$		2X/1X	$\sqrt{S(f_{2X})/S(f_{1X})}$
Wave shape related	Crest Factor	$\frac{\text{Max.}}{\text{RMS}}$	Specific frequency related	(1x–10x)/1x	$(\sum_{n=1}^{10}\sqrt{S(f_{nX})})/\sqrt{S(f_{1X})}$
	Shape Factor	$\frac{\text{RMS}}{\text{Mean}}$		(0–0.39x)/1x	$(\int_{0}^{0.39X}\sqrt{S(f)}df)/\sqrt{S(f_{1X})}$
	Impulse Factor	$\frac{\text{Max.}}{\text{Mean}}$		(0.4x–0.49x)/1x	$(\int_{0.4X}^{0.49X}\sqrt{S(f)}df)/\sqrt{S(f_{1X})}$
				(0.51x–0.99x)/1x	$(\int_{0.51X}^{0.99X}\sqrt{S(f)}df)/\sqrt{S(f_{1X})}$
				(3x–5x)/1x	$(\int_{3X}^{5X}\sqrt{S(f)}df)/\sqrt{S(f_{1X})}$
				(3x, 5x, 7x, 9x)/1x	$(\sum_{n=1}^{4}\sqrt{S(f_{(2n+1)X})})/\sqrt{S(f_{1X})}$

3.1. Omnidirectional regeneration (ODR) of vibration signals

The concept of ODR involves introducing virtual sensors to acquire vibration signals from any arbitrary direction. In most engineering rotor systems, two perpendicular fixed sensors are implemented, as presented in Fig. 3. However, the two acquired signals from the two fixed sensors may not accurately represent the state of the rotor system because an anomaly can happen in a direction that is not line with the sensors. Adding extra sensors often requires the structure of system to be modified and may not always be possible. In contrast, virtual sensors can be placed at any orientation without any physical change to the structure of the system. These virtual sensors can then be used to obtain ODR signals. The ODR signals can then be used to improve the performance of the diagnosis system. Section 3.1.1 defines ODR and Section 3.1.2 explains how ODR signals are validated. In Section 3.1.3, the physical description upon health states of rotors is provided to emphasize the significance of ODR signals.

3.1.1. Definition of ODR

The acquired signals are obtained as a voltage that is inversely proportional to the gap between the sensor and the rotor. The voltage values are transformed into the exact distance by multiplying them by a scale factor, and eliminating the DC component of the voltage returned by the vibration signals. As the shaft rotates, as shown in Fig. 4, the centerline moves from point 1 to point 3, and the distance between the rotor and the actual sensor (c) increases. Accordingly, the vibration signal acquired by the actual sensor (c) moves from point 1 to 3. Signals can also be obtained by the virtual sensors (b) and (d).

The omnidirectional regeneration (ODR) of vibration signals can be regarded as the signals obtained from many virtual sensors placed at any orientation. The ODR signals are actually obtained by transforming the coordinates of the signals from the actual sensors. The rotation about the origin of the Cartesian coordinate system gives a signal at the rotated orientation. In Fig. 4, the virtual sensors are rotated 45 degrees counter-clockwise from the actual sensors. Other virtual sensors can be placed at an orientation of interest by adjusting the rotation angle. This shows that the ODR signals are not new, but are instead hidden signals that may give critical information on the health state of the rotor system.

The principle of ODR is to apply the coordinate rotation in the Cartesian system in a two-dimensional plane. For example, a data point $\boldsymbol{A}$ can be presented in a Cartesian coordinate, as in Fig. 5. The original coordinates, X_0-Y_0, denote the x-position of point $\boldsymbol{A}$ as x_0, and the y-position as y_0. However, the point can be addressed differently when other coordinate systems are used. For example, point $\boldsymbol{A}$ can be denoted as x_1, y_1 from the X_1-Y_1 coordinates in Fig. 5. The coordinates X_1-Y_1 are rotated from the coordinates X_0-Y_0. The relation between the two representations, (x_0,y_0) and (x_1,y_1), can be described as follows:

$$\begin{bmatrix} x_1 \\ y_1 \end{bmatrix} = \begin{bmatrix} \cos\theta & \sin\theta \\ -\sin\theta & \cos\theta \end{bmatrix} \times \begin{bmatrix} x_0 \\ y_0 \end{bmatrix} \tag{3}$$

where θ is the angle between the two coordinate systems in a counter-clockwise rotation. We can apply this principle to a set of scalar values in a time domain. The scalar values x_i and y_i can be replaced by vectors $\boldsymbol{x}_i$ and $\boldsymbol{y}_i$, where $\boldsymbol{x}_i = [x_i(1),x_i(2),\ldots, x_i(n)]$ and $\boldsymbol{y}_i = [y_i(1),y_i(2),\ldots,y_i(n)]$. The scalar values $x_i(k)$ and $y_i(k)$ denote the x- and y-position of the point at time sequence k in the X_i–Y_i coordinate system, respectively. The set of scalar values can describe various types of signals, including vibration. Thus, the vibration signals obtained via proximity sensors can be regarded as $\boldsymbol{x}_0$ and $\boldsymbol{y}_0$. Then, the ODR signals from the nth virtual sensors, $\boldsymbol{x}_n$ and $\boldsymbol{y}_n$, can be defined as:

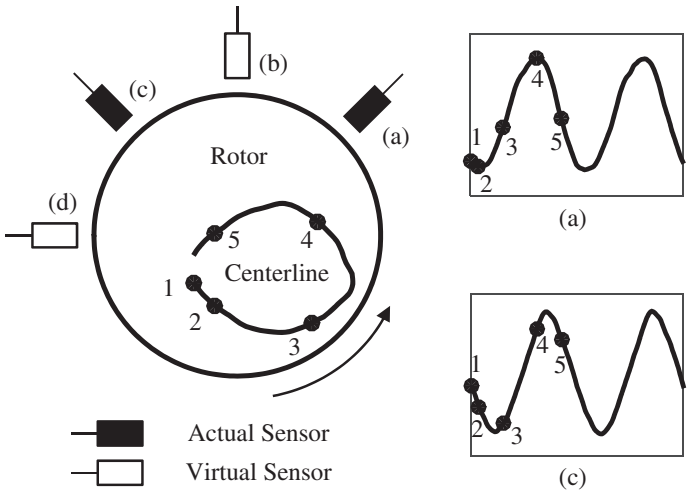

Fig. 4. Actual sensors, (a) and (c), and their signals; virtual sensors, (b) and (d).

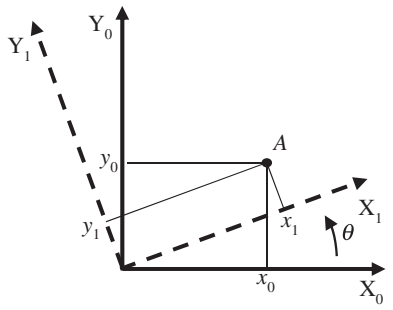

Fig. 5. Coordinate transformation of a point in a two-dimensional system.

$$\begin{aligned} \boldsymbol{x_n} &= \cos(n\Delta\theta)\boldsymbol{x}_0 + \sin(n\Delta\theta)\boldsymbol{y}_0 \\ \boldsymbol{y_n} &= -\sin(n\Delta\theta)\boldsymbol{x}_0 + \cos(n\Delta\theta)\boldsymbol{y}_0 \\ & (n = 1, 2, \ldots, N) \end{aligned} \tag{4}$$

where $\boldsymbol{x}_0$ and $\boldsymbol{y}_0$ are the vibration signals from actual sensors, $\Delta\theta$ is the increment of the rotation angle, and N (= $\pi/\Delta\theta$) is the maximum number of the ODR signals that can be generated.

The ODR can generate vibration signals from any arbitrary direction. Vibration signals around the rotor can be obtained through coordinate transformation by using the incremental angle, $\Delta\theta$. For robust diagnosis of the system health state, $\Delta\theta$ must be carefully determined. However, if $\Delta\theta$ is too small, the computational load will increase due to the increased number of ODR signals (N). Section 3.3 will thus discuss optimal determination of an incremental angle, $\Delta\theta$. In addition, the vibration signals are symmetric about the centerline, so ODR signals within the range of a π rotation angle can be generated. Likewise, there is no need to use both $\boldsymbol{x}_n$ and $\boldsymbol{y}_n$, because the $\boldsymbol{x}_n$ signal is equal to $\boldsymbol{y}_{n+N/2}$, which is the 90° rotated signal of $\boldsymbol{y}_n$. Thus, $\boldsymbol{x}_n$ covers all $\boldsymbol{y}_n$ if the ODR covers more than a half of a rotation.

3.1.2. Validation of ODR signals

The ODR signals are acquired through virtual sensors, as described in Section 3.1.1. To use the ODR signals in the diagnosis process, the ODR signals must be validated. Here, an example using experimental data is provided to validate the ODR method. The two actual sensors and N virtual sensors are placed around half of the circumference, using a constant incremental angle, as shown in Fig. 6. The signal from the ith virtual sensor is denoted as $\boldsymbol{x}_i$, and the signals from actual sensors 1 and 2 are denoted as $\boldsymbol{x}_0$ and $\boldsymbol{y}_0$, respectively.

First, the ODR signal, $\boldsymbol{x}_{N/2}$, should exactly match the actual signal, $\boldsymbol{y}_0$. As shown in Fig. 6, the direction of $N/2$th virtual sensor is equal to that of actual sensor 2, so the signals from the two sensors should be identical. The two vibration signals, $\boldsymbol{x}_{N/2}$ and $\boldsymbol{y}_0$, shown in Fig. 7 prove that they are exactly the same. Second, the direction of the Nth virtual sensor is opposite from the direction of actual sensor 1, so signal $\boldsymbol{x}_N$ should be the inverse of $\boldsymbol{x}_0$. This is also confirmed by the signals shown in Fig. 7. The last evidence is that the orbit formed by the ODR signals, $\boldsymbol{x}_n$ and $\boldsymbol{x}_{n+N/2}$, should retain the same shape as that formed by the actual sensor signals. Using vibration signals from both the actual sensors and the virtual sensors, the orbit shapes are compared in Fig. 8. Although the vibration signals change over the rotation angle, the orbit shape remains the same. From these facts, the ODR signals can be regarded as vibration signals in other directions.

3.1.3. Physical interpretation of the ODR signals

The value of the ODR signals lies within providing the physical information about the health state of rotors in all directions. Some health states such as rubbing and misalignment present inconsistent vibration signal patterns due to the directional nature of rubbing and misalignment. To verify such states being oriented in a certain direction, a simple lumped model for each state is studied. The model consists of a shaft with a disc supported by two journal bearings. To make the model simple, it is assumed that the damping and stiffness only exist at the bearing. In addition, the mass of the shaft as well as the gyroscopic effect of the disc is ignored.

This research views the normal state as the configuration with a bit unbalance. A basic model of isotropic unbalanced rotor is frequently described as follows:

$$M\ddot{x} + C\dot{x} + Kx = mr\omega^2\cos(\omega t + \delta) \tag{5}$$

$$M\ddot{y} + C\dot{y} + Ky = mr\omega^2\sin(\omega t + \delta) \tag{6}$$

where M, C, K are mass, damping, and stiffness respectively, m, r, and δ are unbalance mass, radius, and angular orientation respectively, ω is rotational speed, x and y are lateral displacements of the disc in orthogonal directions as a function of time t [47].

The oil whirl model considers tangential force by fluid. The basic model of oil whirl can be stated as follows:

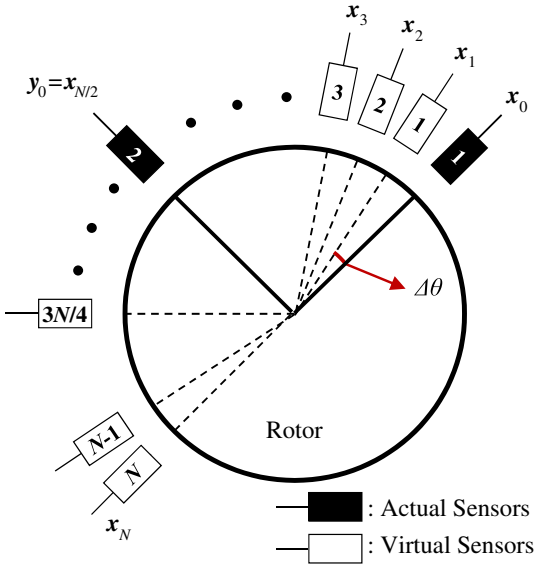

Fig. 6. Diagram of ODR signals.

$$M\ddot{x} + (C + C_f)\dot{x} + Kx + C_f\lambda\omega y = mr\omega^2\cos(\omega t + \delta) \tag{7}$$

$$M\ddot{y} + (C + C_f)\dot{y} + Ky - C_f\lambda\omega x = mr\omega^2\sin(\omega t + \delta) \tag{8}$$

where M, C, K, m, r, δ, ω, x, y denote identical meaning as in Eqs. (5) and (6), C_f is the damping coefficient due to fluid, and λ denotes the ratio between rotor speed and oil circumferential average velocity [47].

The models of rubbing and misalignment states are altered from that of normal and unbalance states. The basic model of partial rubbing is expressed as:

$$M\ddot{x} + C\dot{x} + Kx = mr\omega^2\cos(\omega t + \delta) - F_N(\cos\theta - \mu\sin\theta) \tag{9}$$

$$M\ddot{y} + C\dot{y} + Ky = mr\omega^2\sin(\omega t + \delta) - F_N(\mu\cos\theta + \sin\theta) \tag{10}$$

where M, C, K, m, r, δ, ω, x, y denote the identical meaning as in Eqs. (5) and (6), F_N indicates the normal force, μ is the friction coefficient, and θ is the direction angle of the rubbing part [47].

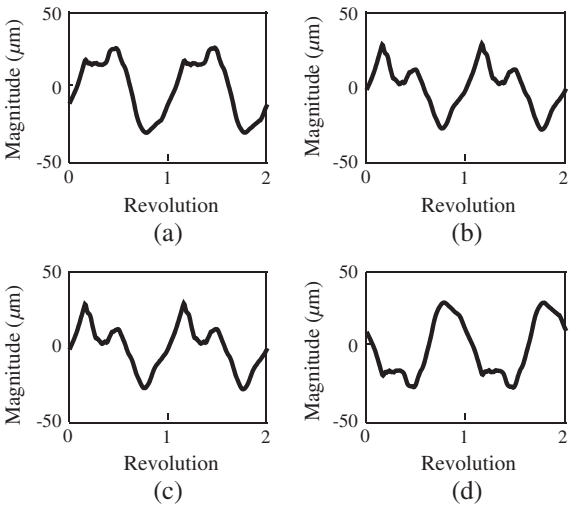

Fig. 7. Two cycles of vibration signals; (a) $\boldsymbol{x}_0$, (b) $\boldsymbol{x}_{N/2}$, (c) $\boldsymbol{y}_0$, and (d) $\boldsymbol{x}_N$.

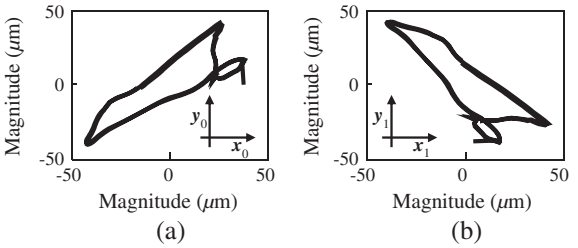

Fig. 8. Orbits by (a) actual sensor signals ($\boldsymbol{x}_0$,$\boldsymbol{y}_0$), and (b) virtual sensor ODR signals ($\boldsymbol{x}_{N/2}$,$\boldsymbol{x}_N$).

Similar physical characteristic can be observed in the basic misalignment model, described as:

$$M\ddot{x} + C\dot{x} + Kx + K_x x^2 = mr\omega^2 \cos(\omega t + \delta) + P\cos\gamma \tag{11}$$

$$M\ddot{y} + C\dot{y} + Ky + K_y y^2 = mr\omega^2 \sin(\omega t + \delta) + P\sin\gamma \tag{12}$$

where M, C, K, m, r, δ, ω, x, y denote the identical meaning as in Eqs. (5) and (6), K_x and K_y are nonlinear stiffness coefficients, P is a radial force due to misaligned rotor, and γ is misaligned direction angle [47]. Using the example system data from [48], the responses are obtained as in Figs. 9–12.

The responses of the normal rotor model, x and y, displays the same vibration signals with a $\pi/2$ phase difference, which indicates that the vibration signals are not direction oriented as in Fig. 9. The behavior of oil whirl also shows little difference between x and y in Fig. 10, but the sub-harmonic frequency component appears due to oil instability. The responses of the rubbing model in Fig. 11 are affected by the direction of rubbing (θ). The misalignment case in Fig. 12 shows different behavior upon the direction of misalignment (γ) as well.

The above stated mathematical models indicate that the external forces of rubbing and misalignment have directional nature, θ and γ. Thus the responses of the two health states depend upon the direction of external forces. Overall, the directional nature in some health states hinders one from correct diagnosis using two gap signals, and this leads to the significance of the ODR signals for robust diagnosis of journal bearing rotor systems.

3.2. Diagnosis of directional faults

Each health state of the rotor system has its own vibration signal characteristics. Among various anomaly states, some states show substantial differences among ODR signals. These states are referred to as directional anomaly states. This implies that vibration signals acquired from the directional anomaly states show remarkable variation over the directional coordinates of the sensors. As stated in Section 3.1.3, the physical characteristics of misalignment and rubbing imply that they can be regarded as directional anomaly states. A misalignment state may exist along two different directional coordinates. An example is shown in Fig. 13. It shows two signal sets of interest for a misalignment state: ($\boldsymbol{x}_{N/4}$,$\boldsymbol{x}_{3N/4}$) and ($\boldsymbol{x}_{2N/4}$,$\boldsymbol{x}_N$). The conventional method, which uses only the measured signals, may give conflicting diagnosis results for the two cases. The variation of the signals due to the directional anomaly states may hurt the robustness of the diagnostic results. Through the directionality check, vibration signals can be classified into directional health states and non-directional anomaly states. The ODR signals can help improve the robustness of diagnostic performance for directional anomaly states because the ODR signals can uncover hidden directional features. On the other hand, non-directional health states have similar vibration signals over rotation angles, as presented in Fig. 14. Since the diagnostic result is independent of the direction of the sensors, the two measured signals can be used for diagnosis, instead of the ODR signals.

For robust diagnosis of directional anomaly states, it is of great importance to correctly determine the directionality of the health states. This metric will work regardless of vibration level and health state. Thus, we propose a directionality metric by making use of the spectral responses of the ODR signals as:

$$D \equiv \frac{Max(S_N(f_{1x})) - Min(S_N(f_{1x}))}{Min(S_N(f_{1x}))} \tag{13}$$

where $S_N(f)$ is the power spectrum set from N ODR signals and f_{1x} is the frequency of the rotating speed. The numerator of the metric (D) is the difference between the maximum and the minimum of the power spectrums at the fundamental frequency among N ODR signals. The denominator is a normalizing constant such that the metric works regardless of different vibration levels and anomaly states. A greater D value indicates a 'directional' anomaly state. Our empirical study finds that a unit value can be used as a threshold to classify 'directional' and 'non-directional' states. This makes sense because the non-directional health states have negligible variation over the directional coordinates of the sensors. Fig. 15 shows the validation study of the metric (D) and the directionality threshold with normal and misalignment health states. As shown in Fig. 15, the metric (D) works well; the directionality of the health states is correctly determined for each of the ten different tests.

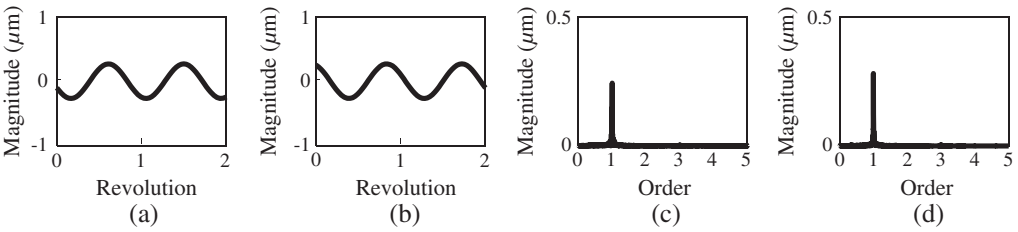

Fig. 9. Two cycle responses of normal state; (a) x, (b) y, and spectral responses of normal state; (c) x, (d) y.

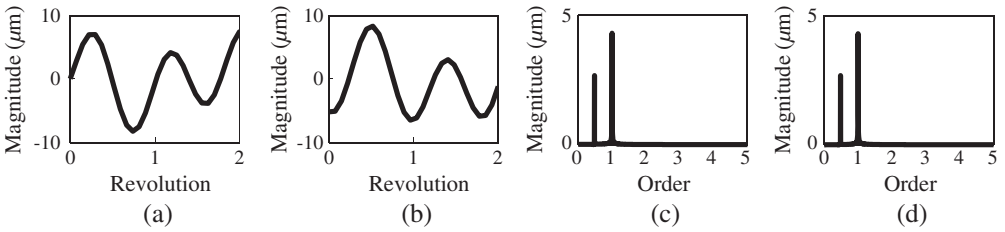

Fig. 10. Two cycle responses of oil whirl state; (a) x, (b) y, and spectral responses of oil whirl state; (c) x, (d) y.

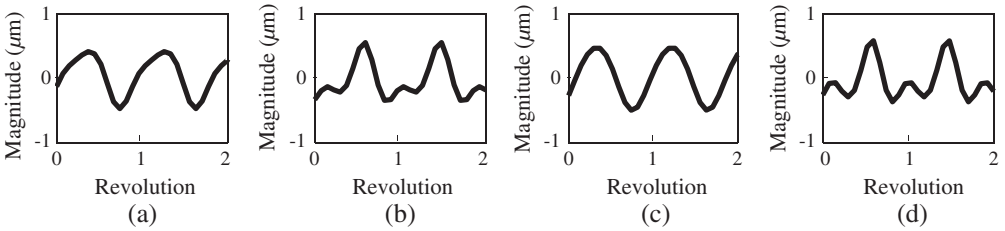

Fig. 11. Two cycle responses of rubbing state; (a) x and (b) y at $\theta = 0°$, (c) x and (d) y at $\theta = 45°$.

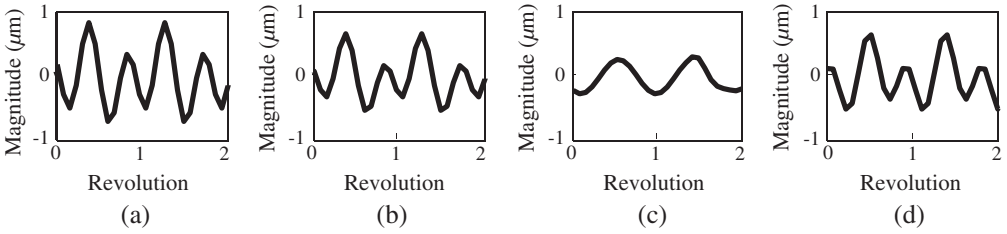

Fig. 12. Two cycle responses of misalignment state; (a) x and (b) y at $\gamma = 0°$, (c) x and (d) y at $\gamma = 45°$.

3.3. Health classification using ODR signals

The directionality metric is used to define whether rotor systems experience directional or non-directional health states. Subject to the result of direction evaluation, one of two different diagnosis procedures can be applied, as shown in Fig. 16. For directional health states, all ODR signals are used for feature generation because the characteristics of a directional health state appear in a certain direction. For every ODR signal, features are generated as described in Section 2.2.1, and then classification is performed using the generated features. Consequently, the class prediction gives N number of results for a unit time of the health state. To transform the N number of results into a single class prediction, a majority voting scheme is implemented for the final classification procedure.

Here, an example of the majority voting scheme is applied to a misalignment state. The number of virtual sensors, N, is set to sixteen, as shown in Fig. 6. The class is predicted for each of sixteen ODR signals, which gives sixteen predictions, as shown in Table 2. Among the sixteen results, the misalignment outnumbers the others, thus the final state is predicted as misalignment.

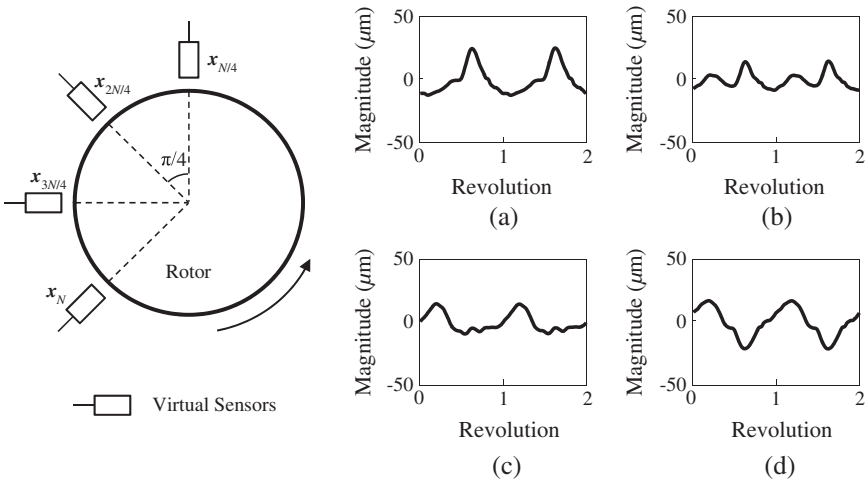

Fig. 13. ODR signals of the misalignment state; (a) $\boldsymbol{x}_{N/4}$, (b) $\boldsymbol{x}_{2N/4}$, (c) $\boldsymbol{x}_{3N/4}$, and (d) $\boldsymbol{x}_N$.

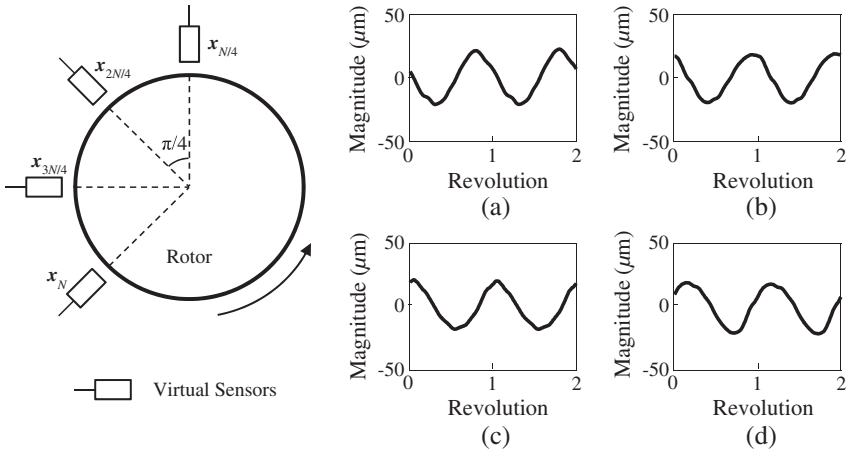

Fig. 14. ODR signals of the normal state; (a) $\boldsymbol{x}_{N/4}$, (b) $\boldsymbol{x}_{2N/4}$, (c) $\boldsymbol{x}_{3N/4}$, and (d) $\boldsymbol{x}_N$.

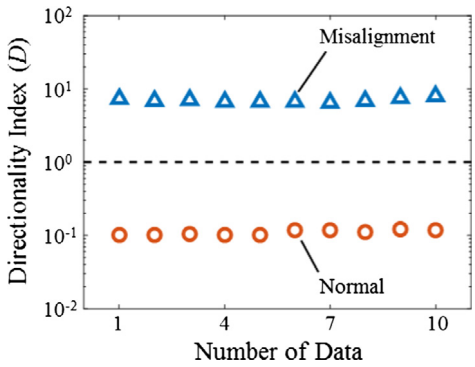

Fig. 15. Example of a direction evaluation result.

In contrast to the directional health states, non-directional ones follow the approach used in conventional supervised learning methods, as presented in Fig. 16. Since the non-directional health states show similar vibration signals over rotation angles, a signal from the actual sensor is used for the feature generation and classification procedures.

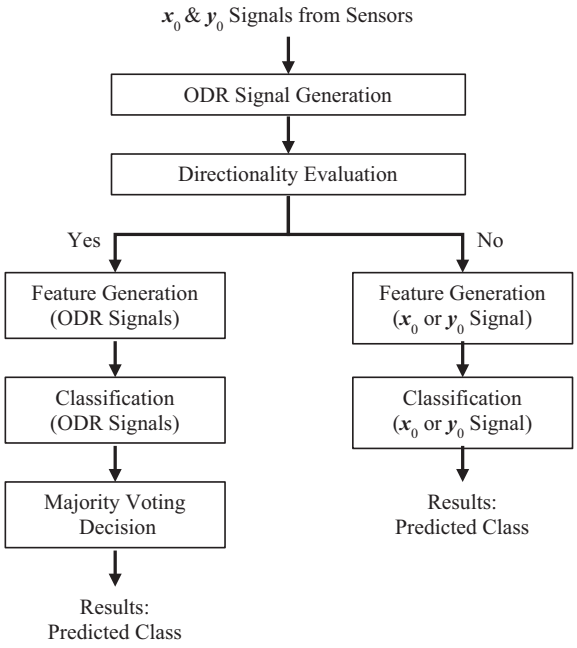

Fig. 16. Health classification using ODR signals.

4. Validation for ODR-based diagnosis

The objective of this section is to show the validation process used to demonstrate the effectiveness of the ODR signals for robust diagnosis of journal bearing rotor system health states. This validation study was conducted using the RK4 testbed, as described in Section 2.1.1. Section 4.1 describes the configuration of the testbed and the signals of each health state. Section 4.2 includes the results of directionality evaluation using the metric, *D*. In Sections 4.3 and 4.4, the signals of non-directional and directional health states are analyzed, respectively. Finally, the robustness of ODR-based diagnosis is validated by classification in Section 4.5.

4.1. Description of health states

This section describes the health states that were used to validate the robustness of ODR-based diagnosis. As stated in Section 2.1.1, five health states—normal, oil whirl, misalignment, rubbing, and rubbing with unbalance—were tested. Each test was performed for sixty seconds and was repeated. To consider the uncertainty of test settings, all test-bed parts were reassembled before every test was conducted. A total of three data sets, each set comprising five health states, were used for the validation.

The normal health state is defined as a system with only a small amount of unbalance. Through the balancing procedure, the rms of the 2nd bearing signal was set as 10 μm at 3600 rpm. The measured signals follow a simple sinusoidal wave shape. Also, the vibration signals from actual gap sensors are similar to each other in terms of the shape and amplitude. This indicates that the normal state is a non-directional health state. The oil whirl state is another non-directional health, state since the oil in the bearings affects the rotor system around the entire circumference of the rotor. The instability of the oil was introduced in the testbed by using the oil whirl kit of the RK4, which controls the pressure of the oil supply. At the tran-

Table 2
Example of predicted class using ODR signals.

ODR signals	Predicted class	ODR signals	Predicted class
$\boldsymbol{x}_1$	Misalignment	$\boldsymbol{x}_9$	Misalignment
$\boldsymbol{x}_2$	Misalignment	$\boldsymbol{x}_{10}$	Misalignment
$\boldsymbol{x}_3$	Misalignment	$\boldsymbol{x}_{11}$	Misalignment
$\boldsymbol{x}_4$	Misalignment	$\boldsymbol{x}_{12}$	Misalignment
$\boldsymbol{x}_5$	Misalignment	$\boldsymbol{x}_{13}$	Rubbing
$\boldsymbol{x}_6$	Normal	$\boldsymbol{x}_{14}$	Rubbing
$\boldsymbol{x}_7$	Normal	$\boldsymbol{x}_{15}$	Misalignment
$\boldsymbol{x}_8$	Normal	$\boldsymbol{x}_{16}$	Rubbing with Unbalance

sient states, the pressure was raised to a certain level to prevent oil whip. Only at the 3600 rpm steady-state, was the pressure dropped and the oil whirl anomaly state was created. The signals in Fig. 17b were acquired from the gap sensors in the oil whirl kit. The misalignment state was tested by shifting the shorter shaft downwards using a customized jig. Since the shaft was shifted in one direction, this state can be grouped as a directional health state. The measured signals shown in Fig. 17c also indicate that shaft rotation is affected by the direction of the shift. The two signals are very different in terms of the shape and amplitude. Each test was performed after a balancing procedure, and was run at a 3600 rpm steady-state. The rubbing state, precisely impact-rubbing, is another directional health state. The testbed setting was exactly same as that of the normal state, but the rubbing was implemented by forcing the rubbing screw to contact the shaft near the 2nd bearing. The screw partially contacts during a cycle of rotation, which can be viewed as an impact. The two measured signals show difference in shape and amplitude, and the rubbing effect is reflected as the cut at the peak. The rubbing test was also done after the balancing procedure. In addition to the rubbing state, a "rubbing with unbalance" test was performed independently. The rubbing with unbalance test is the same as the rubbing test except a greater unbalance weight is attached to the disc. After balancing the rotor system to the normal state defined above, 15 g·mm of unbalance weight was added. The rubbing was then implemented at the steady state of 3600 rpm. The measured signals show similar shape to those of the rubbing state, but the rubbing with unbalance case shows a greater amplitude. Thus, this state can also be viewed as a directional health state.

Overall, the test configurations define the normal and the oil whirl as non-directional health states, while the other three states were defined as directional health states. This was mathematically confirmed in Section 3.1.3. In Section 4.2, the directionality of each health state is evaluated by the metric defined in Section 3.2.

4.2. Directionality of health states

The effectiveness of the directionality evaluation metric, D, was validated using the test-bed data. D was evaluated for every sixty cycles (one second) of vibration signal, as stated in Section 2.2.1. Each test was sixty-seconds long, so sixty data were evaluated for each test, as shown in Fig. 18. The evaluation results of three data sets are shown in Fig. 18a, b, and c. The dotted line is the unit value, which splits directional and non-directional states.

The test results of all three sets validate the effectiveness of directionality. The D values of the normal and the oil whirl states are less than one, which indicates a non-directional health state. In contrast, the D values of the other health states are

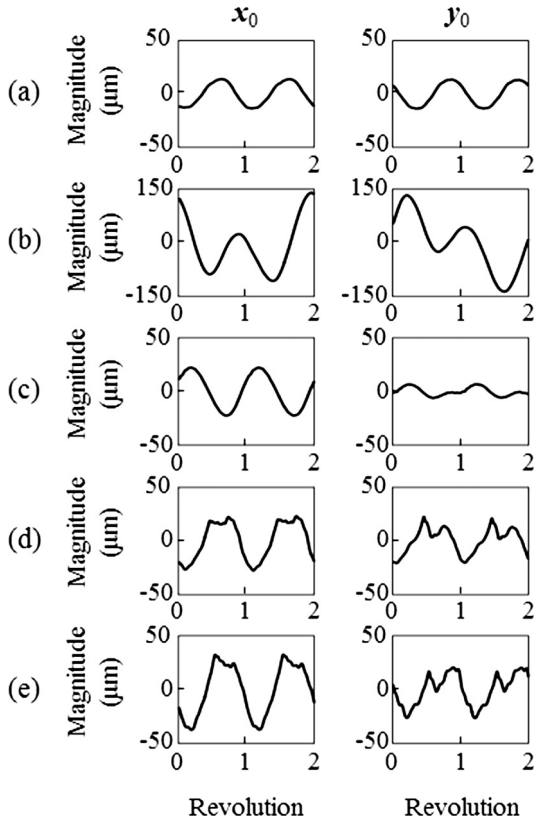

Fig. 17. Signals of health states from actual sensors.

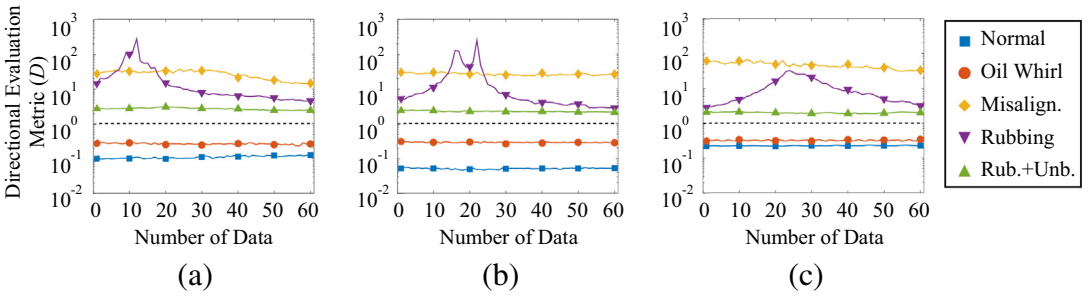

Fig. 18. Results of the directional evaluation metric for (a) set 1, (b) set 2, and (c) set 3.

greater than one, which implies a directional health state. These results confirm that the directionality evaluation metric (D), and its threshold, can define the directionality of health states.

4.3. Measured signals of non-directional health states

This section analyzes the vibration signals of the non-directional health states studied: normal and oil whirl. The measured signals of normal and oil whirl health states from the actual sensors are shown in Fig. 19a and b, respectively. In the frequency domain, the time signals are transformed by Fast Fourier Transform (FFT). The FFT plots of the normal state confirm that a 1X fundamental frequency is dominant. The total orbit shape also confirms the normal state. In addition, the directionality can be roughly estimated by the 1X orbit shape, since the difference between the length of major and minor axes is not large. From these facts, the normal state can be estimated as a non-directional health state.

The oil whirl health state shows fluctuating time signals, but its FFT plots point out the typical oil whirl characteristic, which is the harmonic component under the fundamental frequency. Theoretically, 0.42–0.48X the fundamental frequency is sensed, as shown in Fig. 19b [49–51]. Though the time signals look very different from each other, the FFT plots have similar responses. Additionally, the orbit of 1X signals is close to a circle, which indicates a non-directional health state.

The two non-directional health states can be diagnosed using any of the measured or ODR signals because the signals do not vary much over the rotation. Thus, rather than using multiple ODR signals, which produce redundant features, only the measured signals are used for classification of the non-directional health states. This will be discussed further in Section 4.5.

4.4. ODR signals of directional health states

The vibration signals of directional health states are analyzed in this section. First, in the misalignment health state, there is a large difference between the $\boldsymbol{x}_0$ and $\boldsymbol{y}_0$ signals, as shown in Fig. 20. Both the time and FFT plots in Fig. 20a denote significant variation. This is mainly due to the shifted shaft in the horizontal direction, which leads to the increase in horizontal stiffness of the bearing. The directional dependency is clearly recognizable in the 1X orbit plot. The difference between the major and minor axes is substantial, which leads to a significant value of the directionality metric, D. In addition, the 1X orbit ODR signals, as well as the $\boldsymbol{y}_0$ signal, were affected by the directional nature, as shown in Fig. 21a.

For the rubbing health state, signals change greatly over the rotation angle. Among the four signals, $\boldsymbol{x}_0$, $\boldsymbol{y}_0$, $\boldsymbol{x}_{N/4}$, and $\boldsymbol{x}_{3N/4}$ shown in Figs. 20b and 21b, only $\boldsymbol{y}_0$ and $\boldsymbol{x}_{N/4}$ have relatively large harmonics of fundamental frequency in FFT plots, which

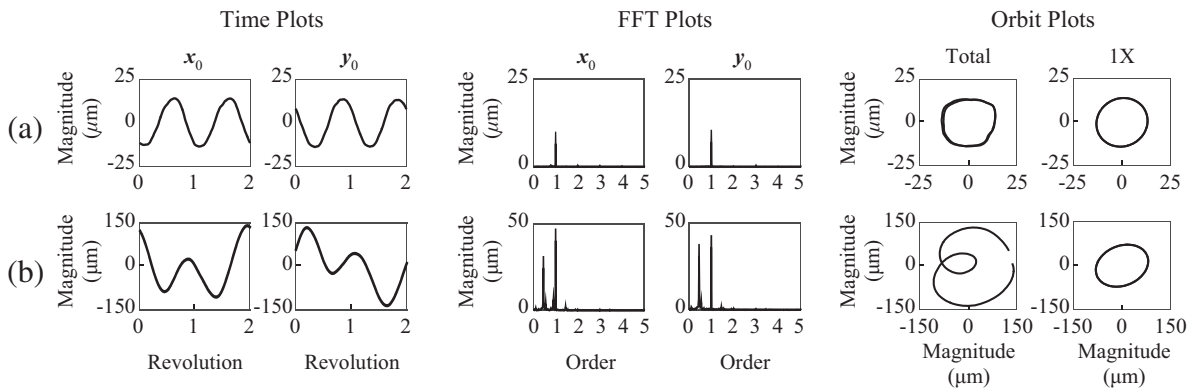

Fig. 19. Time, FFT, and orbit plots of measured signals; (a) normal and (b) oil whirl state.

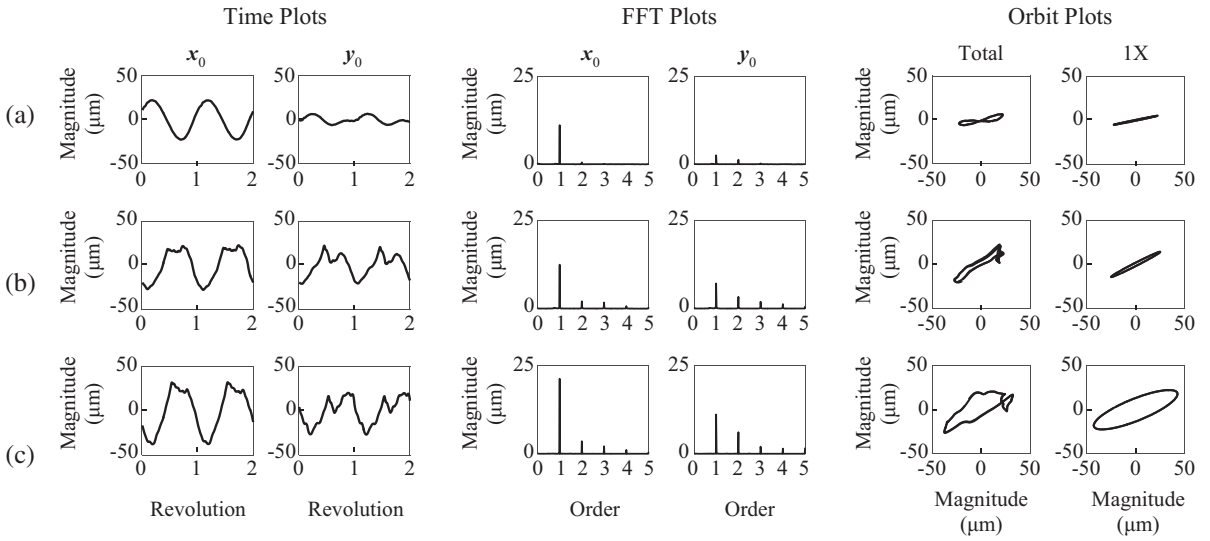

Fig. 20. Time, FFT, and orbit plots of measured signals; (a) misalignment, (b) rubbing, and (c) rubbing with unbalance.

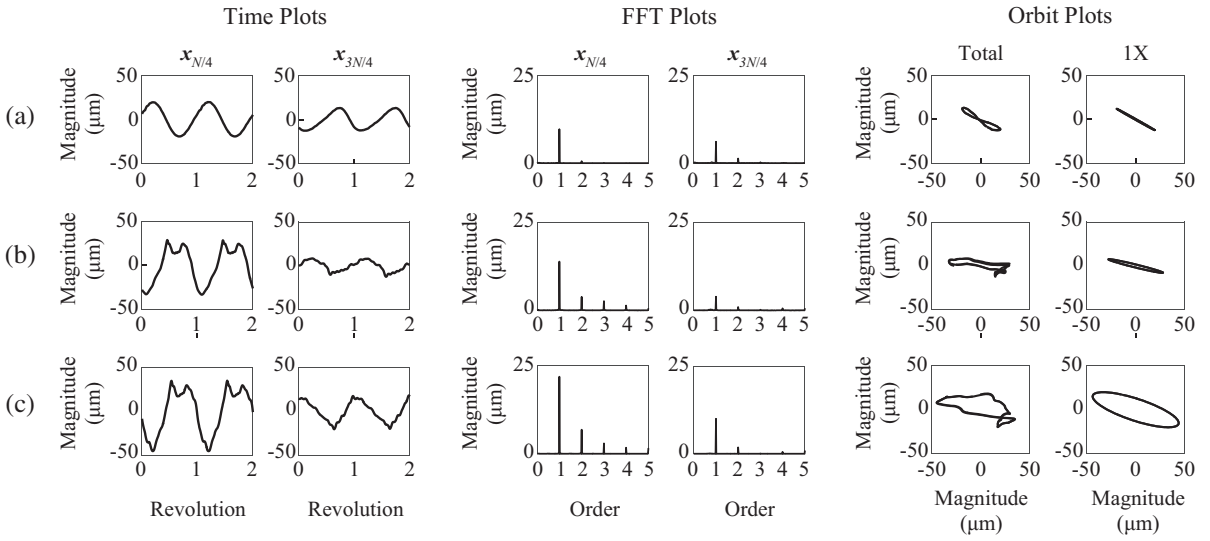

Fig. 21. Time, FFT, and orbit plots of ODR signals; (a) misalignment, (b) rubbing, and (c) rubbing with unbalance.

can be regarded as a rubbing state. The sinusoidal signals of $\boldsymbol{y}_0$ and $\boldsymbol{x}_{N/4}$ in time plots are obviously trimmed due to impact-rubbing. However, the effect of impact-rubbing is weakly observed in the other signals. Moreover, the time plots are all different from each other, which explicitly shows directional dependency.

The signals of the "rubbing with unbalance" state are similar to those of the rubbing state. The amplitude of the 1X component in FFT was increased, as compared to that of the rubbing state. This is revealed in the time plots as well. It is observed in the orbit plot of the 1X component in FFT that the difference between major and minor axes is decreased due to the imbalance added to the rubbing state. The D value thus becomes smaller than that of the rubbing states.

4.5. Classification

To validate the effectiveness of ODR signals on directional health states, the class prediction result using ODR signals was compared to that without using ODR signals. In addition, the results for the non-directional health state are also included.

The five health states were grouped into either directional or non-directional states. For the directional state group, the features were extracted from all ODR signals. Using the extracted features, the classifier was trained, and prediction was performed for the unlabeled data. Since N results were obtained for each sixty-cycle data, the final prediction result was

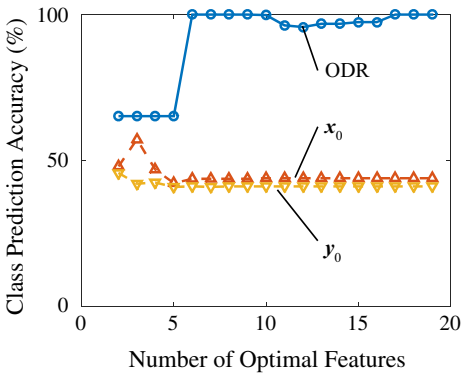

Fig. 22. Classification results of directional health states using measured signals.

obtained by a majority voting process. For the non-directional state group, the features were extracted from one of the measured signals. The ODR signals were not used for this group because the time and frequency features do not change much as compared to those found in directional states. Using the extracted features, the training and prediction processes were then performed.

First, the effectiveness of the ODR method can be validated by examining the results shown in Fig. 22 for directional health states. The class prediction accuracy of ODR and non-ODR signals is compared in the figure. The lines marked by circles represent the results from the proposed ODR method, while the lines marked by upward- and downward-triangles represent the results obtained using non-ODR signals. For both cases, the optimal number of features (n) for the feature selection process (as described in Section 2.2.1), was increased from two to nineteen. Each line represents an average of three cross validation cases by three data sets. The results obtained by using ODR signals are based on the majority voting scores of sixteen ODR signals ($\Delta\theta = 11.25°$), as described in Section 3.3. In contrast to these results, the other lines show the results of the use of non-ODR signals, where only the measured signals, $\boldsymbol{x}_0$ and $\boldsymbol{y}_0$, where used for training and prediction.

The classification results clearly show that the ODR method outperforms the conventional method that uses the $\boldsymbol{x}_0$ and $\boldsymbol{y}_0$ signals separately. When six or more features are used, the ODR method classifies the given data with prediction accuracy greater than 98%. In contrast, the results from using only $\boldsymbol{x}_0$ and $\boldsymbol{y}_0$ signals show less than fifty-percent accuracy for most of the feature numbers. These results indicate that $\boldsymbol{x}_0$ and $\boldsymbol{y}_0$ cannot fully characterize directional health states. In addition, the class prediction results derived using $\boldsymbol{x}_n$ signals are presented in Fig. 23. To consider the uncertainty of directions, all possible combinations of signals for prediction were used with $\boldsymbol{x}_0$ and $\boldsymbol{y}_0$ training. Since N signals were generated by ODR, N^3 combinations for three health states were used for the prediction. The average of N^3 results are presented as lines marked by triangles.

As expected, the prediction accuracies of the ODR method are substantially higher than those of the non-ODR method. Most of the predictions by the ODR method reach an accuracy of one hundred percent when the number of optimal features was larger than five. In contrast, the average accuracy of the non-ODR method remains less than fifty percent, irrespective of optimal features. The ODR method, when five or less optimal features are used, shows about a seventy percent accuracy due to misclassification of the "rubbing with unbalance" case. This misclassification is eliminated after amplitude-related features were included in the optimal features. Finally, as shown in Fig. 23, accuracies of the non-ODR combinations had accu-

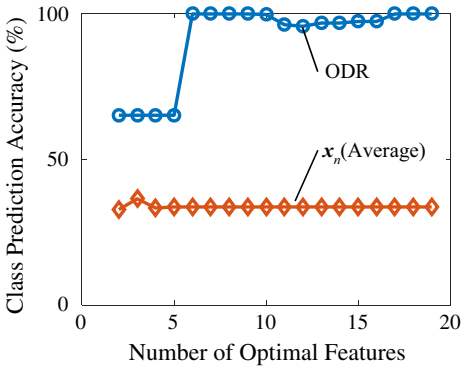

Fig. 23. Classification results of directional health states: Average of all feasible combinations.

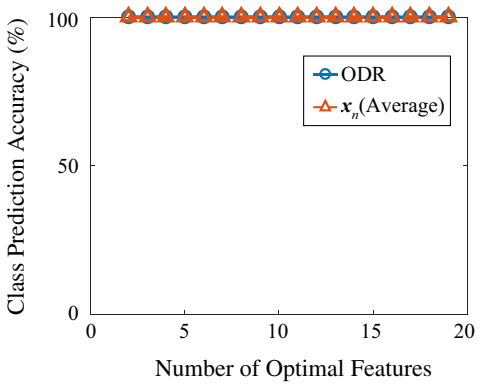

Fig. 24. Classification results of non-directional health states: Average of all feasible combinations.

racies between zero and one hundred percent. This means that prediction accuracy heavily depends on the direction of the abnormality and the sensors.

Second, the class prediction results for non-directional health states are shown in Fig. 24. The class prediction accuracy of ODR and non-ODR is also presented in the figure. Similar to the directional case, the ODR method uses N ODR signals for training and prediction, whereas the non-ODR method uses only one signal. The non-ODR results are the average prediction accuracy of N^3 combinations. The results indicate that both the ODR method and the non-ODR method are valid for classification of non-directional health states. Not much difference exists between the ODR method and the non-ODR method because signals do not vary with respect to direction. Thus, if the health states are grouped as non-directional by the evaluation metric, a signal from any direction can be used for the training and prediction processes.

5. Conclusion

The main goal of this research was to enhance the performance of diagnosis algorithms for journal bearing rotor systems by considering the direction of the sensors and the anomaly sources. Little research to date has tried to determine the direction of anomaly states by quantifying orbit shape and using full-spectrum analysis. However, neither of the previous methods were robust to characterize the physical interpretations of the rotors. In contrast, the ODR signal based method proposed here considers vibration signals in all directions; this method has sufficient physical interpretations for accurate health prediction. Also, the proposed ODR method follows a general supervised learning process, which makes it easier to apply to other systems as well.

In this research, the proposed ODR method was demonstrated using data acquired from a testbed. Five health states from the testbed were grouped into either directional or non-directional states using a directionality metric. The presence of directionality of each health state was shown with mathematical models. By applying a supervised learning based ODR method to the directional group, health states were accurately diagnosed. However, when the traditional method was used and the ODR method was not applied, the classification results were inconsistent. Overall, accuracies varied from zero percent to one hundred percent because the direction of the sensors and the anomaly sources did not always match. These results clearly show that for robust diagnosis of journal bearing rotor systems, the direction of the health state must be considered.

For non-directional states, the conventional method that only uses acquired signals also achieved high accuracy. The normal and oil whirl states had less variations in features over ODR rotations, as compared to those of directional states. Thus, applying the ODR method to non-directional states will only increase the computational load while achieving the same classification accuracy. Therefore, the directionality metric of the health state should be first evaluated and the ODR method should be used when the metric indicates a directional health state (e.g., $D > 1$). To enable use of the proposed diagnosis algorithm with less computational load for practical use, directionality evaluation is of great importance.

In this study, the proposed ODR method was demonstrated using experimental data. Due to the limited configurations of the testbed, five health states in steady-state conditions were examined. Additional health states such as crack and seal rubbing, may be considered in future work. Also for further research, the number of ODR signals, N, can be optimized considering the prediction accuracy and the computational load.

Acknowledgement

This work was supported by the Technology Innovation Program (10050980, System Level Reliability Assessment and Improvement for New Growth Power Industry Equipment) funded by the Ministry of Trade, Industry & Energy (MI, Korea).

References

[1] A. Kusiak, A. Verma, A data-driven approach for monitoring blade pitch faults in wind turbines, IEEE Trans. Sust. Energy 2 (2011) 87–96.
[2] S.M. Namburu, M.S. Azam, J. Luo, K. Choi, K.R. Pattipati, Data-driven modeling, fault diagnosis and optimal sensor selection for HVAC chillers, IEEE Trans. Automat. Sci. Eng. 4 (2007) 469–473.
[3] B.D. Youn, P. Kyung Min, H. Chao, Y. Joung Taek, K. Hee Soo, J. Beom Chan, et al, Statistical health reasoning of water-cooled power generator stator bars against moisture absorption, IEEE Trans. Energy Convers., 30, 2015, pp. 1376–1385.
[4] C. Hu, B.D. Youn, P. Wang, J. Taek Yoon, Ensemble of data-driven prognostic algorithms for robust prediction of remaining useful life, Rel. Eng. Syst. Safety 103 (2012) 120–135, 7.
[5] P. Wang, B.D. Youn, C. Hu, J.M. Ha, B. Jeon, A probabilistic detectability-based sensor network design method for system health monitoring and prognostics, J. Intell. Mater. Syst. Struct. (2014), p. 1045389X14541496.
[6] C. Hu, B.D. Youn, T. Kim, P. Wang, A co-training-based approach for prediction of remaining useful life utilizing both failure and suspension data, Mech. Syst. Signal Process. 62–63 (2015) 75–90, 10.
[7] C. Hu, P. Wang, B.D. Youn, W.-R. Lee, J.T. Yoon, Copula-based statistical health grade system against mechanical faults of power transformers, IEEE Trans. Power Deliv. 27 (2012) 1809–1819.
[8] P.D. McFadden, M.M. Toozhy, Application of synchronous averaging to vibration monitoring of rolling element bearings, Mech. Syst. Signal Process. 14 (2000) 891–906, 11.
[9] J.M. Ha, B.D. Youn, H. Oh, B. Han, Y. Jung, J. Park, Autocorrelation-based time synchronous averaging for condition monitoring of planetary gearboxes in wind turbines, Mech. Syst. Signal Process. 70–71 (2016) 161–175, 3.
[10] F. Bonnardot, M. El Badaoui, R. Randall, J. Daniere, F. Guillet, Use of the acceleration signal of a gearbox in order to perform angular resampling (with limited speed fluctuation), Mech. Syst. Signal Process. 19 (2005) 766–785.
[11] L.F. Villa, A. Reñones, J.R. Perán, L.J. De Miguel, Angular resampling for vibration analysis in wind turbines under non-linear speed fluctuation, Mech. Syst. Signal Process. 25 (2011) 2157–2168.
[12] T. Han, B.-S. Yang, W.-H. Choi, J.-S. Kim, Fault diagnosis system of induction motors based on neural network and genetic algorithm using stator current signals, Int. J. Rotating Mach. 2006 (2006) 13.
[13] B.-S. Yang, K.J. Kim, Application of Dempster-Shafer theory in fault diagnosis of induction motors using vibration and current signals, Mech. Syst. Signal Process. 20 (2006) 403–420.
[14] B. Samanta, K.R. Al-Balushi, Artificial neural network based fault diagnostics of rolling element bearings using time-domain features, Mech. Syst. Signal Process. 17 (2003) 317–328, 3.
[15] J. Sanz, R. Perera, C. Huerta, Fault diagnosis of rotating machinery based on auto-associative neural networks and wavelet transforms, J. Sound Vib. 302 (2007) 981–999, 5/22.
[16] B. Liu, Adaptive harmonic wavelet transform with applications in vibration analysis, J. Sound Vib. 262 (2003) 45–64, 4/17.
[17] T. Ramesh Babu, S. Srikanth, A.S. Sekhar, Hilbert–Huang transform for detection and monitoring of crack in a transient rotor, Mech. Syst. Signal Process. 22 (2008) 905–914, 5.
[18] Q. Gao, C. Duan, H. Fan, Q. Meng, Rotating machine fault diagnosis using empirical mode decomposition, Mech. Syst. Signal Process. 22 (2008) 1072–1081, 7.
[19] B.M. Ebrahimi, J. Faiz, S. Lotfi-fard, P. Pillay, Novel indices for broken rotor bars fault diagnosis in induction motors using wavelet transform, Mech. Syst. Signal Process. 30 (2012) 131–145, 7.
[20] B. Samanta, Gear fault detection using artificial neural networks and support vector machines with genetic algorithms, Mech. Syst. Signal Process. 18 (2004) 625–644, 5.
[21] V. Sugumaran, V. Muralidharan, K.I. Ramachandran, Feature selection using decision tree and classification through proximal Support Vector Machine for fault diagnostics of roller bearing, Mech. Syst. Signal Process. 21 (2007) 930–942, 2.
[22] S. Theodoridis, K. Koutroumbas, Pattern recognition–Fourth ed., Academic Press, 2009.
[23] S. Verron, T. Tiplica, A. Kobi, Fault detection and identification with a new feature selection based on mutual information, J. Process Control 18 (2008) 479–490, 6.
[24] B.A. Paya, I.I. Esat, M.N.M. Badi, Artificial neural network based fault diagnostics of rotating machinery using wavelet transforms as a preprocessor, Mech. Syst. Signal Process. 11 (1997) 751–765, 9.
[25] L.H. Chiang, M.E. Kotanchek, A.K. Kordon, Fault diagnosis based on Fisher discriminant analysis and support vector machines, Comput. Chem. Eng. 28 (2004) 1389–1401, 7/15.
[26] S.-W. Fei, X.-B. Zhang, Fault diagnosis of power transformer based on support vector machine with genetic algorithm, Expert Syst. Appl. 36 (2009) 11352–11357, 10.
[27] M. Saimurugan, K.I. Ramachandran, V. Sugumaran, N.R. Sakthivel, Multi component fault diagnosis of rotational mechanical system based on decision tree and support vector machine, Expert Syst. Appl. 38 (2011) 3819–3826, 4.
[28] A. Widodo, B.-S. Yang, Support vector machine in machine condition monitoring and fault diagnosis, Mech. Syst. Signal Process. 21 (2007) 2560–2574.
[29] S.-F. Yuan, F.-L. Chu, Support vector machines-based fault diagnosis for turbo-pump rotor, Mech. Syst. Signal Process. 20 (2006) 939–952, 5.
[30] J. Li, P. Cui, Improved kernel fisher discriminant analysis for fault diagnosis, Expert Syst. Appl. 36 (2009) 1423–1432, 3.
[31] C. Yan, H. Zhang, H. Li, Y. Li, W. Huang, Automatic identification of shaft orbits for steam turbine generator sets, in: WRI Global Congress on Intelligent Systems, 2009. GCIS '09, 2009, pp. 53–57.
[32] H. Wang, H. Wang, Y. Ji, Orbit identification method based on ISOMAP for rotor system fault diagnosis, in: 2013 IEEE 11th International Conference on Electronic Measurement & Instruments (ICEMI), 2013, pp. 668–671.
[33] N. Bachschmid, P. Pennacchi, A. Vania, Diagnostic significance of orbit shape analysis and its application to improve machine fault detection, J. Brazilian Soc. Mech. Sci. Eng. 26 (2004) 200–208.
[34] F. Bo, Z. Jian-Zhong, C. Wen-Qing, Y. Bing-Hui, Identification of the shaft orbits for turbine rotor by modified Fourier descriptors, in: Proceedings of 2004 International Conference on Machine Learning and Cybernetics, 2004, vol. 2, 2004, pp. 1162–1167.
[35] C. Yan, H. Zhang, L. Wu, Automatic recognition of orbit shape for fault diagnosis in steam turbine generator sets, J. Comput. Inform. Syst. 6 (2010) 1995–2008.
[36] C. Wang, J. Zhou, P. Kou, Z. Luo, Y. Zhang, Identification of shaft orbit for hydraulic generator unit using chain code and probability neural network, Appl. Soft Comput. 12 (2012) 423–429, 1.
[37] W. Fengqi, G. Meng, Compound rub malfunctions feature extraction based on full-spectrum cascade analysis and SVM, Mech. Syst. Signal Process. 20 (2006) 2007–2021, 11.
[38] X. Zhao, T.H. Patel, M.J. Zuo, Multivariate EMD and full spectrum based condition monitoring for rotating machinery, Mech. Syst. Signal Process. 27 (2012) 712–728, 2.
[39] P. Goldman, A. Muszynska, Application of full spectrum to rotating machinery diagnostics, Orbit 20 (1999) 17–21.
[40] T.H. Patel, A.K. Darpe, Experimental investigations on vibration response of misaligned rotors, Mech. Syst. Signal Process. 23 (2009) 2236–2252, 10.
[41] I. Standard, Mechanical Vibration-Evaluation of Machine Vibration by Measurements on Non-Rotating Parts, ISO/IS 10816, 1996.
[42] F. Bonnardot, R. Randall, J. Antoni, F. Guillet, Enhanced unsupervised noise cancellation using angular resampling for planetary bearing fault diagnosis, Int. J. Acoust. Vib. 9 (2004) 51–60.
[43] B. Jeon, J. Jung, B. Youn, Y.-W. Kim, Y.-C. Bae, Datum unit optimization for robustness of a journal bearing diagnosis system, Int. J. Precision Eng. Manuf. 16 (2015) 2411–2425, 2015/10/01.

[44] O. Ludwig, U. Nunes, Novel maximum-margin training algorithms for supervised neural networks, IEEE Trans. Neural Networks 21 (2010) 972–984.
[45] H.-C. Kim, S. Pang, H.-M. Je, D. Kim, S. Yang Bang, Constructing support vector machine ensemble, Pattern Recognit. 36 (2003) 2757–2767, 12.
[46] C.-C. Chang, C.-J. Lin, LIBSVM: a library for support vector machines, ACM Trans. Intell. Syst. Technol. 2 (2011) 1–27.
[47] A. Muszynska, Rotordynamics, CRC Press, 2005.
[48] B.O. Al-bedoor, Transient torsional and lateral vibrations of unbalanced rotors with rotor-to-stator rubbing, J. Sound Vib. 229 (2000) 627–645.
[49] K.N. Gupta, Vibration — a tool for machine diagnostics and condition monitoring, Sadhana 22 (1997) 393–410, 1997/06/01.
[50] Y. Wu, S. Li, S. Liu, H.-S. Dou, Z. Qian, Vibration-based condition monitoring, in: Vibration of Hydraulic Machinery, Springer, 2013, pp. 431–477.
[51] Y. Lei, Z. He, Y. Zi, Application of the EEMD Method to Rotor Fault Diagnosis of Rotating Machinery, vol. 23, Mechanical Systems and Signal Processing, 2009, 5.